



Title	Lubricated Sliding of a Rigid Cylinder on a Viscoelastic Half Space
Author(s)	Wu, Haibin; Jagota, Anand; Hui, Chung-Yuen
Citation	Tribology letters, 70(1), 1 https://doi.org/10.1007/s11249-021-01537-4
Issue Date	2022-03
Doc URL	http://hdl.handle.net/2115/88187
Rights	This version of the article has been accepted for publication, after peer review (when applicable) and is subject to Springer Nature 's AM terms of use, but is not the Version of Record and does not reflect post-acceptance improvements, or any corrections. The Version of Record is available online at: https://doi.org/10.1007/s11249-021-01537-4
Type	article (author version)
File Information	Tribol. Lett. 70-1.pdf



[Instructions for use](#)

Lubricated sliding of a rigid cylinder on a viscoelastic half space

Haibin Wu¹, Anand Jagota², Chung-Yuen Hui^{1,3#}

¹ Department of Mechanical and Aerospace Engineering, Field of Theoretical and Applied Mechanics, Cornell University, Ithaca, NY 14853, USA

² Departments of Bioengineering and of Chemical & Biomolecular Engineering, 111 Research Drive, Lehigh University, Bethlehem, PA 18015, USA

³ Global Station for Soft Matter, GI-CoRE, Hokkaido University, Sapporo, Japan

#Corresponding author: Chung-Yuen Hui, ch45@cornell.edu

Abstract

We study the lubricated sliding of a rigid cylinder on a viscoelastic half space with a single characteristic retardation time. Besides the generalized inverse Hersey number β , which is the sole parameter governing elastic lubrication, the viscoelastic lubrication solution depends on two additional dimensionless parameters: α and f . α is the characteristic retardation time divided by the time for the rigid cylinder to move one contact width and f determines the strength of viscoelasticity. We have developed a numerical scheme to solve this viscoelastic lubrication problem. Our numerical results show that the total friction force can be decomposed into viscoelastic and hydrodynamic components. The viscoelastic component of the friction is well approximated by the dry limit in which the liquid layer is all squeezed out and the resistance to sliding is due entirely to viscoelastic dissipation. The hydrodynamic limit is well approximated by a modification of the elastic limit in which friction is due entirely to hydrodynamics. We also study the dependence of the hydrodynamic pressure, film thickness and the friction coefficient on these parameters.

Keywords Soft lubrication · Viscoelasticity · Energy dissipation · Hydrodynamic friction · Contact

1. Introduction

Lubricated sliding, in which a thin liquid film separates two solids in relative motion, is ubiquitous, e.g., in the smooth operation of gears and pistons in machines and joints in our bodies. In the past decade or so, applications of lubricated sliding has expanded from stiff-stiff contact, such as in bearings [1, 2] and pistons [3, 4], to applications that involve stiff-soft or soft-soft contact, such as in rubber bearings and seals [5–8] and rubber tires to road contact [9, 10]. Many studies also have examined lubricated sliding of elastic contact with a sphere-on-fat or cylinder-on-fat contact geometry to investigate the effects of properties such as material modulus, lubricant viscosity and surface roughness [11–19].

As one of the intense research subject, Elasto-hydrodynamic lubrication (EHL) has been studied for a long time. In EHL, the materials are assumed to be elastic. However, most soft materials such as elastomers, gels or cartilage are viscoelastic. Viscoelasticity cause energy dissipation which significantly increases friction during lubricated sliding. Compared to EHL, viscoelastic-hydrodynamic lubrication (VEHL)

has received much less attention, partly because of the difficulty of simultaneously solving the nonlinear Reynolds equation for the fluid phase and the history-dependent equations of viscoelasticity for the solid. Because of this difficulty, literature on this subject is scant, as noted by Putignano [20], who recently developed a numerical method to solve this class of problems.

A *special* case of VEHL is “dry” sliding, where the fluid layer is absent (or completely squeezed out) and solid-solid contact is itself frictionless. Thus, in “dry” sliding, the sliding resistance is due entirely to viscoelastic dissipation. Hunter [21] studied the sliding contact of a rigid cylinder with viscoelastic half space and obtained an exact formula for the contact pressure and contact width. Carbone [22] extended Hunter’s result to address a similar sliding problem on a finite viscoelastic layer using a more realistic viscoelastic model. Additional numerical and experimental research on this topic can be found in [7, 23, 24].

The problem of a lubricated rigid cylinder sliding on a viscoelastic substrate have been studied by Herrebrugh[25], Dowson[26], Hooke and Huang [27], Elsharkawy [28], Scaraggi [29], Putignano [20, 23, 30, 31] and others [13, 18, 32]. These works have focused on issues such as the general effect of material viscoelasticity on the lubrication process and the analytical solution of some simplified viscoelastic lubrication geometries. However, previous work has not addressed the relationship between the mechanics of viscoelastic hydrodynamic lubrication and simpler cases of elasto-hydrodynamic lubrication and the pure dry sliding contact. Hui et. al. [33] recently showed that the full VEHL solution of a cylinder sliding on a thin viscoelastic foundation can be decomposed, to a good approximation, into a combination of the corresponding dry sliding and the EHL solutions. Whether this decomposition is obtained in the more general VEHL problem of lubricated sliding on a viscoelastic half-space remains an open question, and this is the main focus of the work presented here.

Specifically, we study the problem of lubricated sliding of a rigid cylinder on a soft viscoelastic half space. As pressure-sensitivity of viscosity is negligible for typical soft lubrication conditions [34], we assume lubricant to be iso-viscous, i.e., Newtonian with constant viscosity. In our previous works [35, 36], we have found that with appropriate normalization the EHL problem is governed by a single parameter β which is a generalized version of the inverse Hersey number [11]. For soft contacts β is typically much larger than 1. Including the viscoelasticity of the substrate introduces two additional dimensionless parameters α, f , which are the normalized loading rate and the normalized strength of the retardation spectrum. We study the nature of the solution over large ranges of these parameters to investigate how they affect features of the solution such as hydrodynamic pressure, liquid film thickness, and the friction force.

The plan for the remainder of this paper is as follows: Section 2 summarizes the formulation of the VEHL problem. In this section, two special cases are studied in detail. One is the dry sliding case where the liquid layer is absent, and second one is the EHL problem where viscoelasticity is not considered. We show that these two cases approximately constitute two important components of the full problem. Section 3 presents the detailed numerical recipes to solve the full VEHL problem. We highlight some findings that cause numerical difficulties especially for the cylinder problem where the displacement is not well defined. Section 4 presents the numerical results and comparison with the existing theory. Results are presented in the form of a generalized Stribeck surface. We conclude with a summary and discussion in Section 5.

Nomenclature

R	Radius of the cylinder
η	Liquid layer viscosity
V	Sliding velocity of the cylinder
N	Vertical line force on the cylinder
ν	Poisson ratio of the substrate, $\nu \approx 1/2$ in this work.
E_0^*	$E_0^* = \frac{E_0}{1-\nu^2}$
E_∞^*	$E_\infty^* = \frac{E_\infty}{1-\nu^2}$
a_0	$a_0 \equiv \left(\frac{4NR}{\pi E_\infty^*} \right)^{1/2}$, the half contact width of a cylinder on an <i>elastic</i> solid without sliding, subjected to a line force N .
x, \bar{x}	x coordinate in the moving frame, $\bar{x} = x/a_0$ is the normalized x coordinate
y	y coordinate in the moving frame
h, \bar{h}	The profile of cylinder, $\bar{h} = hR/a_0^2$
h_0, \bar{h}_0	$h(x=0)$, the indentation depth of the cylinder, $\bar{h}_0 = h_0R/a_0^2$
w, \bar{w}	substrate surface deformation, $\bar{w} = wR/a_0^2$
u, \bar{u}	liquid film thickness, $u(x) = h(x) - w(x)$, $\bar{u} = uR/a_0^2$
t	time
p	Hydrodynamic pressure
$C(t)$	Creep function in tension test;
E_0	instantaneous Young's modulus
E_∞	Long term Young's modulus
τ	characteristic retardation time
f	strength of retardation spectrum, $f = \frac{E_0}{E_\infty} - 1$
p_{Hertz}	pressure distribution of the classical elastic "Hertz contact"
α	$\alpha = \frac{a_0}{V\tau}$, the ratio of the time to slide a Hertz contact length to the retardation time of the viscoelastic substrate.
β	$\beta = \frac{4N^2}{3\pi^2\eta VE_\infty^* R}$, the inverse generalized Hersey number
β^*	$\beta^* \equiv \beta(1 + fe^{-1.41\alpha})$
Ei	$Ei(x) = \int_{-\infty}^x \frac{e^t}{t} dt$, the exponential integral function
τ_{yx}	Shear stress component in liquid
v_x	fluid velocity in the horizontal direction
F_h	Friction force due to hydrodynamics, $\bar{F}_h = \frac{R}{Na_0} F_h$

μ_h	friction coefficient, $\mu_h = F_h / N$ due to hydrodynamic flow
F_v, \bar{F}_v	Friction force due to viscoelasticity of substrate, $\bar{F}_v = \frac{R}{Na_0} F_v$
μ_v	friction coefficient due to viscoelastic dissipation, $\mu_v = F_v / N$
x_1	The position of contact leading edge in dry sliding
x_2	The position of contact trailing edge in dry sliding
a, \bar{a}	a is the semi-contact width in dry sliding, $\bar{a} = a / a_0$
b, \bar{b}	\bar{b} is the x coordinate of the contact midpoint in dry sliding, $\bar{b} = b / a_0$
k	$k = (1 + f) \alpha \bar{a}$
I_0, I_1	modified Bessel function of the first kind
K_0, K_1	modified Bessel function of the second kind
c	Integration constant
$A_i, B_i,$	Coefficients of the discretized Reynolds equation
C_i, D_i	
χ_{ik}	Substrate surface deformation at \bar{x}_i due to a unit line load at \bar{x}_k
λ_p	Relaxation factor for updating \bar{p} in the relaxation method
$\lambda_{h1}, \lambda_{h2}$	Relaxation factors for updating \bar{h}_0 in the relaxation method
n_h	The frequency of \bar{h}_0 updates in the numerical iteration scheme;
F_{tot}	Total friction force $F_{tot} = F_v + F_h; \bar{F}_{tot} = \frac{R}{Na_0} F_{tot}$
μ_{tot}	Total friction coefficient; $\mu_{tot} = \mu_v + \mu_h$

2. Theoretical Methods

2.1 Problem statement and theoretical formulation

A schematic of lubricated sliding of a rigid circular cylinder on viscoelastic half space is shown in Fig.1. The rigid cylinder is assumed to be infinitely long in the out-of-plane direction. The radius of the cylinder is R . Between the rigid cylinder and the viscoelastic half space, there exists a thin liquid layer of constant viscosity η . The cylinder is moving with a constant velocity V to the right under the application of a horizontal line force F . A constant vertical line force N is imposed on the cylinder. A coordinate system (x, y) is attached to the moving cylinder. In this moving coordinate frame, the vertical position of the cylinder is $h(x)$ and at $x = 0$, $h_0 \equiv h(0)$. The substrate is deformed under the hydrodynamic pressure and the deformed surface is denoted by $w(x)$. The liquid film thickness is $u(x) = h(x) - w(x)$.

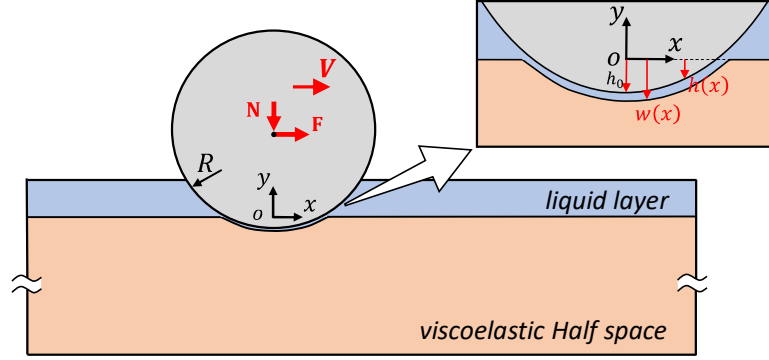


Fig.1 a schematic of lubricated sliding of a rigid cylinder on a viscoelastic half space

The deformation in the half space is under plane strain, where the out-of-plane displacement is zero and the in-plane stress and strain fields are independent of the out-of-plane coordinate. As is well known, in plane strain, the displacement field has a logarithmic singularity at infinity. As a result, the surface displacement w and h_0 are only defined to within an arbitrary constant. Here we follow the standard procedure to determine this constant: we chose a point on the surface at distance r_0 far from the cylinder as a datum for normal displacement w and h_0 . Details are given below.

In steady sliding, all the fields are independent of time t in the moving frame (x,y) even though the material is rate-dependent. Specifically, the material time derivative of field quantities in a stationary frame can be converted to spatial derivative in the moving frame, both in the fluid or in the viscoelastic solid. For details, please see SI. The Reynolds equation for the lubrication layer is [37]:

$$\left(\frac{p_{,x}(h-w)^3}{12\eta} \right)_{,x} = - \left(\frac{V}{2} \right) (h_{,x} - w_{,x}) \quad (1)$$

where p is the hydrodynamic pressure and a comma denotes differentiation. Since the “effective contact region” is usually much smaller than the cylinder radius, the circular profile of cylinder is approximated as a parabola, i.e.,

$$h = h_0 + \frac{x^2}{2R} \quad (2)$$

The substrate is assumed to be a standard viscoelastic solid where there is a single characteristic retardation time τ . Specifically, the creep function $C(t)$ in simple tension is

$$C(t) = E_0^{-1} \left[1 + f(1 - e^{-t/\tau}) \right] \quad (3)$$

where E_0 is the instantaneous Young’s modulus and f is the strength of retardation spectrum; f is related to the long and short time Young’s modulus E_∞, E_0 by

$$f = \frac{E_0}{E_\infty} - 1 \quad (4)$$

For highly viscoelastic solids such as rubber, $f \approx 10^3$ [38]. For a purely elastic solid, $f = 0$. We assume that the Poisson ratio of the half space, ν , is a constant independent of time, which is a good approximation for soft solids which are almost incompressible; $\nu \approx 1/2$.

The vertical surface displacement $w(x)$ due to a normal pressure distribution $p(x)$ was given by Hunter [21]:

$$w(x) = \frac{2}{\pi E_0^*} \left[\int_{-\infty}^{+\infty} p(x') \ln|x-x'| dx' + f \int_0^\infty e^{-\xi} d\xi \int_{-\infty}^{+\infty} p(x') \ln|x+V\tau\xi-x'| dx' \right] + const \quad (5)$$

where $E_0^* = \frac{E_0}{1-\nu^2}$ is the instantaneous plane strain modulus. Note that $p(x)$ is the hydrodynamic fluid pressure acting on the substrate surface. It is positive when the fluid is in compression. The term $w|_{x=0}$ is always negative in the coordinate frame shown in Fig.1. The first integral in Eq.(5) is the elastic displacement (for an elastic substrate with E_0 and ν). The double integral in Eq.(5) accounts for viscoelasticity. When $f=0$ ($E_0=E_\infty$), we recover the elastic solution. As noted above, the constant in Eq. 3 indicates that w cannot be determined uniquely. Force balance indicates that the overall hydrodynamic pressure should balance the normal applied line load, i.e.,

$$\int_{-\infty}^{+\infty} p(x) dx = N \quad (6)$$

Finally, we note that the stress and strain must vanish at infinity; in particular, the material far away from the cylinder is elastic with *relaxed* modulus E_∞ .

2.1.1 Normalization

We normalize location of material point, x , by the ‘‘Hertz contact length’’ a_0 , which is the half contact width of a cylinder on an *elastic* solid without sliding, subjected to a line force N . The Young’s modulus and Poisson’s ratio of this reference elastic solid are denoted by E_∞, ν , respectively. The half-contact length a_0 and the pressure distribution of the classical elastic ‘‘Hertz contact’’ are given by Eqs.(7,8) [39].

$$a_0 \equiv \left(\frac{4NR}{\pi E_\infty^*} \right)^{1/2}, E_\infty^* = \frac{E_\infty}{1-\nu^2} \quad (7)$$

$$p_{Hertz} = \begin{cases} \frac{2N}{\pi a_0} \sqrt{1 - \left(\frac{x}{a_0} \right)^2}, & |x| < a_0 \\ 0, & |x| \geq a_0 \end{cases} \quad (8)$$

We normalize the hydrodynamic pressure p by $\max(p_{Hertz})$. The normalization of each variable is:

$$\bar{x} = \frac{x}{a_0}, \quad \bar{h} = \frac{Rh}{a_0^2} = \bar{h}_0 + \frac{1}{2}\bar{x}^2, \quad \bar{w} = \frac{Rw}{a_0^2}, \quad \bar{p} = \frac{\pi a_0}{2N} p \quad (9)$$

The normalized form of Eqs.(1), (5) and (6) are:

$$\beta \left[\bar{p}_{,\bar{x}} (\bar{h} - \bar{w})^3 \right]_{,\bar{x}} = -(\bar{h}_{,\bar{x}} - \bar{w}_{,\bar{x}}) \quad (10)$$

$$\bar{w}(\bar{x}) = \frac{1}{\pi(1+f)} \left[\int_{-\infty}^{+\infty} \bar{p}(\bar{x}') \ln|\bar{x} - \bar{x}'| d\bar{x}' + f \int_0^{\infty} e^{-\xi} d\xi \int_{-\infty}^{+\infty} \bar{p}(\bar{x}') \ln \left| \bar{x} + \frac{1}{\alpha} \xi - \bar{x}' \right| d\bar{x}' \right] + const \quad (11)$$

$$\int_{-\infty}^{+\infty} \bar{p}(\bar{x}) d\bar{x} = \frac{\pi}{2} \quad (12)$$

$$\alpha = \frac{a_0}{V\tau} \quad (13)$$

$$\beta = \frac{E_{\infty}^* a_0^4}{12\eta VR^3} = \frac{4N^2}{3\pi^2 \eta E_{\infty}^* R} \quad (14)$$

Note β in Eq.(10) is the inverse generalized Hersey number. Large β indicates either larger normal force or smaller sliding velocity. α is the ratio of the time to slide a Hertz contact length to the retardation time of the viscoelastic substrate. When $\alpha \rightarrow 0$, the viscoelastic material behaves elastically with modulus E_0 as the material is fully unrelaxed, while for $\alpha \rightarrow \infty$ the material is fully relaxed and behaves as an elastic solid with Young's modulus E_{∞} . For intermediate values of α , the substrate dissipates energy. Here we note that β is typically very large for soft material sliding. As an example, in an experiment of recent study[35] where $R=2mm$, $E_{\infty}^*=10^5 Pa$, $\eta=5.1Pa \cdot s$, $N=119mN/mm$, $V=1mm/s$, $\beta \approx 1.8 \times 10^3 \gg 1$.

2.1.2 Substrate deformation

For most electrohydrodynamic lubrication simulations, the evaluation of the substrate deformation ranks as the most computationally-demanding part of the entire simulation process [40–42], followed by the process of solving of the Reynolds equation and checking the force balance condition. For VEHL, the evaluation of substrate deformation is even more difficult since the deformation depends on the loading history. This difficulty is reflected by the double integral in Eq.(11). Therefore, it is important to find an efficient way to evaluate the viscoelastic deformation of substrate. By changing the integration order of \bar{x} (space) and ξ (time) in the 2nd part of RHS of Eq.(6b), we convert the double integral in Eq.(11) into a single integral Eq.(15), which can be evaluated much more efficiently:

$$\bar{w}(\bar{x}) = \frac{1}{\pi} \int_{-\infty}^{+\infty} \bar{p}(\bar{x}') \ln|\bar{x} - \bar{x}'| d\bar{x}' - \frac{f}{\pi(1+f)} \int_{-\infty}^{+\infty} \bar{p}(\bar{x}') e^{\alpha(\bar{x}-\bar{x}')} Ei(-\alpha(\bar{x}-\bar{x}')) d\bar{x}' + const \quad (15)$$

where $Ei(x)$ is the exponential integral function, $Ei(x) = \int_{-\infty}^x \frac{e^t}{t} dt$. Details on the derivation of Eq.(15) is given in the Supporting information (SI). The constant in Eq.(15) is determined by selecting a datum at $\bar{x} = \bar{r}_0$ where $\bar{w}(\bar{r}_0) = 0$ for $f=0$. Physically, it corresponds to the case that when the substrate is fully relaxed, the vertical displacement is zero at $\bar{x} = \bar{r}_0$. The constant in Eq.(15) is:

$$const = -\frac{1}{\pi} \int_{-\infty}^{+\infty} \bar{P}(\bar{x}') \ln|\bar{r}_0 - \bar{x}'| d\bar{x}' \quad (16)$$

In our problem, \bar{r}_0 is selected to be large enough so it lies in the relaxed region. The final expression for the vertical displacement is:

$$\bar{w}(\bar{x}) = \frac{1}{\pi} \int_{-\infty}^{+\infty} \bar{P}(\bar{s}) \ln \left| \frac{\bar{x} - \bar{s}}{\bar{r}_0 - \bar{s}} \right| d\bar{s} - \frac{f}{\pi(1+f)} \int_{-\infty}^{+\infty} P(\bar{s}) e^{\alpha(\bar{x}-\bar{s})} Ei(-\alpha(\bar{x}-\bar{s})) d\bar{s} \quad (17)$$

2.1.3 Friction force due to hydrodynamics and viscoelasticity

Friction during lubricated sliding results from two sources. The first is due to shear flow of the liquid layer while the second is due to viscoelastic dissipation which causes the hydrodynamic pressure to be skewed.

The friction F_h due to hydrodynamics can be obtained by integrating the shear traction τ_{yx} in the fluid layer. For a Newtonian fluid, τ_{yx} is related with the strain rate $\partial v_x / \partial y$ by:

$$\tau_{yx} = \eta \frac{\partial v_x}{\partial y} \quad (18)$$

where $v_x(x)$ is the component of the fluid velocity in the horizontal direction. Following [36]:

$$v_x(x, y) = \left[\frac{p_x}{2\eta} (y-h) + \frac{v}{h-w} \right] (y-w). \quad (19)$$

Integrating the shear traction $\tau_{yx}|_{y=h}$ over the entire domain gives

$$F_h = \int_{-\infty}^{\infty} \tau_{yx}|_{y=h} dx = \frac{Na_0}{R} \int_{-\infty}^{\infty} \left[\frac{\bar{p}_{,\bar{x}} \bar{u}}{\pi} + \frac{1}{3\pi\beta\bar{u}} \right] d\bar{x} \equiv \frac{Na_0}{R} \bar{F}_h \quad (20)$$

The friction coefficient μ_h that corresponds to F_h is defined as $\mu_h \equiv F_h / N$ and is given by

$$\mu_h = \frac{a_0}{R} \int_{-\infty}^{\infty} \left[\frac{\bar{p}_{,\bar{x}} \bar{u}}{\pi} + \frac{1}{3\pi\beta\bar{u}} \right] d\bar{x} \quad (21)$$

Next, we consider the friction force F_v due to viscoelastic dissipation. When the substrate is viscoelastic, the hydrodynamic pressure is generally skewed. This skewed pressure distribution gives rise to a net horizontal force which results in a friction force F_v . A schematic figure illustrating this mechanism is in Fig.2.

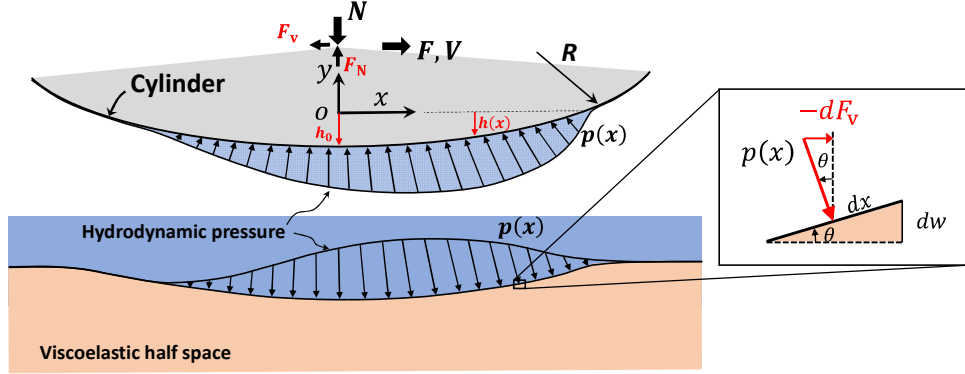


Fig.2 Schematic figure showing how viscoelasticity causes a skewed hydrodynamic pressure, which leads to friction force F_v .

Figure 2 shows the free body diagram of the cylinder and the viscoelastic half space. The friction force is the integral of $dF_v = -p(x)\sin\theta dx$ over the entire domain, where the negative sign represents the direction of F_v pointing to the right and $\sin\theta \simeq dw / dx$. Therefore,

$$F_v = -\int_{-\infty}^{+\infty} p(x)\sin\theta dx = -\int_{-\infty}^{+\infty} p(x)\frac{dw}{dx} dx = -\int_{-\infty}^{+\infty} p(x)dw = -\frac{Na_0}{R} \frac{2}{\pi} \int_{-\infty}^{+\infty} \bar{p}(x)d\bar{w} \equiv \frac{Na_0}{R} \bar{F}_v \quad (22)$$

The friction coefficient μ_v is

$$\mu_v \equiv \frac{F_v}{N} = -\frac{2a_0}{\pi R} \int_{-\infty}^{+\infty} \bar{p}(x)d\bar{w} \quad (23)$$

2.2 Two limiting cases: Drying Sliding and EHL

A recent study by Hui et. al. [33] has shown that the friction force during viscoelasto-hydrodynamic lubrication can be well approximated as a combination of two simpler cases: the dry sliding case where the liquid is absent and the lubricated sliding case where the substrate is elastic. However, the substrate in that work was modeled as a viscoelastic spring foundation in which mechanical interactions are purely local, in the sense that the displacement of the substrate at a point is affected by the pressure only at that point. This is in general not a good assumption for a substrate that is large in extent compared with all relevant dimensions. Here we study the feasibility of a similar decomposition

for lubricated sliding of a rigid cylinder on a viscoelastic half space. These two limiting cases are considered in the next two sections (2.2.1) and (2.2.2).

2.2.1 Dry Sliding

In the absence of a liquid film, the cylinder slides on the viscoelastic half space with solid-to-solid contact. We call this case *dry sliding*. A schematic of dry sliding is shown in Fig.3. In it, the liquid film thickness $u(x) \equiv h(x) - w(x) = 0$ so $h(x) = w(x)$ everywhere. In particular, the pressure must vanish at the leading and trailing contact edges, which we denote by x_1 and x_2 , respectively. That is, $p(x_1) = p(x_2) = 0$. In Fig. 3, a is the semi-contact width and b is the x coordinate of the contact midpoint. The solution of this problem was obtained by Hunter [11]. Here we adopt his solution to study the relevant mechanics. It must be noted that, because by supposition physical contact between the surfaces bears no shear traction, the friction force in dry sliding is due entirely to viscoelastic dissipation [11].

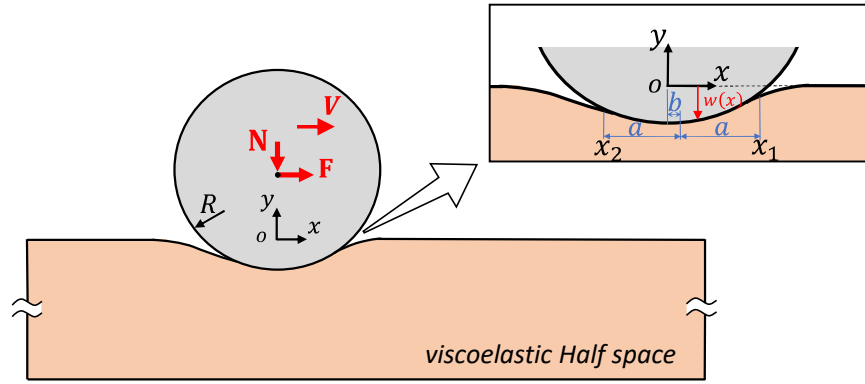


Fig.3 a schematic of dry sliding of a rigid cylinder on a viscoelastic half space

The pressure distribution is given by Hunter [11]. Using our normalization, it is

$$\bar{p}(\bar{x}) = \begin{cases} k\bar{a} \cdot e^{\frac{k(\bar{x}-\bar{b})}{\bar{a}}} \int_{(\bar{x}-\bar{b})/\bar{a}}^1 e^{-k\xi} \left\{ \sqrt{1-\xi^2} + \frac{(\bar{\Gamma}_2 - \bar{\Gamma}_1 \xi)}{\sqrt{1-\xi^2}} \right\} d\xi, & \bar{x}_2 \leq \bar{x} \leq \bar{x}_1 \\ 0, & \text{elsewhere} \end{cases} \quad (24)$$

where:

$$k = (1+f)\alpha\bar{a} \quad (25)$$

$$\bar{a}^2 \equiv \left(\frac{a}{a_0} \right)^2 = \frac{K_0(\alpha\bar{a})/K_1(\alpha\bar{a}) + I_0(k)/I_1(k)}{K_0(\alpha\bar{a})/K_1(\alpha\bar{a}) + I_0(k)/I_1(k) + 2f/k} \quad (26)$$

$$\bar{\Gamma}_1 = -\frac{1}{k} - \frac{1}{2} \left(\frac{1}{\bar{a}^2} - 1 \right) \frac{I_0(k)}{I_1(k)} \quad (27)$$

$$\bar{\Gamma}_2 = \frac{1}{2} \left(\frac{1}{\bar{a}^2} - 1 \right) \quad (28)$$

$$\bar{b} \equiv \frac{b}{a_0} = \bar{\Gamma}_1 + \frac{1}{\alpha \bar{a}} \quad (29)$$

$$\bar{x}_1 = \bar{a} + \bar{b}, \quad \bar{x}_2 = \bar{b} - \bar{a} \quad (30)$$

In Eq.(26) I_0 , I_1 and K_0 , K_1 are the modified Bessel function of the first and second kind respectively. The normalized semi-contact width \bar{a} is determined by the numerical solution of the transcendental equation Eq.(26). Once \bar{a} is determined, Eqs. (27-29) can be used to determine $\bar{\Gamma}_1, \bar{\Gamma}_2$ and \bar{b} . In the SI, we show that for the special cases where $\alpha \rightarrow 0$ or $\alpha \rightarrow \infty$, one recovers the classical elastic Hertz solution.

We use Eq.(23) and Eq.(24) to determine the dry friction force F_v . Since in dry sliding the deformed surface's curvature is the same as the cylinder's surface curvature, $\sin\theta \approx \frac{dw}{dx} = \frac{x}{R}$ for $x_2 \leq x \leq x_1$. The dry sliding friction F_v and the friction coefficient μ_v are:

$$F_v = -\int_{x_2}^{x_1} p(x) \frac{x}{R} dx = \frac{Na_0}{R} \left[\bar{b} - \frac{1}{\alpha(1+f)} - \bar{a}^3 \bar{\Gamma}_1 \right] \equiv \frac{Na_0}{R} \bar{F}_v \quad (31)$$

$$\mu_v = \frac{F_v}{N} = \frac{a_0}{R} \left[\bar{b} - \frac{1}{\alpha(1+f)} - \bar{a}^3 \bar{\Gamma}_1 \right] \quad (32)$$

2.2.2 Lubricated Sliding with an Elastic Substrate (special case, $f=0$ or $\alpha=\infty$)

Next, we consider the special case of an elastic substrate. For this case, $f=0$ or $\alpha=\infty$, and the solution depends on a single parameter β . Integrating both sides of the Reynolds equation, Eq.(10), gives:

$$\beta \bar{p}_{,\bar{x}} \bar{u}^3 = -\bar{u} + c. \quad (33)$$

The constant of integration c depends only on β and is the normalized thickness where the pressure gradient is exactly zero. A scaling analysis (see the Supporting information) shows that for $\beta \gg 1$, Eq.(13) holds when $c = O(1/\sqrt{\beta})$ and $\bar{u} = O(1/\sqrt{\beta})$. To validate this scaling analysis, we numerically solved Eq.(33) together with (Eq.15 with $f=0$) to determine c and the pressure distribution. Details of these calculations are given in SI. We found

$$c = \frac{0.197}{\sqrt{\beta}} + \frac{0.951}{\beta}. \quad (34)$$

Figure 4 shows that Eq.(34) agrees very well with the numerical values of c for $\beta \geq 50$. The error is less than 20% even at $\beta=10$.

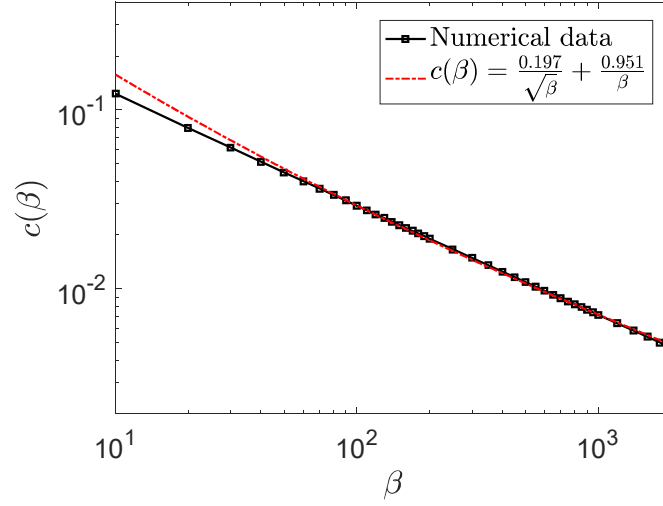


Fig.4 Comparison of $c(\beta)$. Numerical result are symbols (the line is to guide the eyes) and the scaling result of Eq.(34).

To obtain the hydrodynamic friction (see Eq.20), we need both the pressure and film thickness distribution. As expected, the pressure distribution for large β is almost identical to the Hertz pressure (see SI), which is

$$\bar{p}(\bar{x}) = \begin{cases} \sqrt{1-\bar{x}^2}, & -1 < \bar{x} < 1 \\ 0, & \text{elsewhere} \end{cases} \quad (35)$$

The fact that normalized pressure distribution vanishes rapidly outside $[-1,1]$ allows us to replace the integration limits in Eq.(20) from -1 to 1. An approximate expression for the liquid film thickness \bar{u} in the interval $|\bar{x}| < 1$ can be obtained using Eqs.(33) and (34), this results in (for details, see SI):

$$\bar{u} \approx c(\beta)(1 + a_1\bar{x} + a_2\bar{x}^2) = \left(\frac{0.197}{\sqrt{\beta}} + \frac{0.951}{\beta} \right) \left(1 + (0.197)^2 \cdot \bar{x} + 3 \times (0.197)^4 \cdot \bar{x}^2 \right) \quad |\bar{x}| < 1 \quad (36)$$

Figure 5 shows that the numerical film thickness profiles for $\beta=1000$ and $\beta=2000$ are in excellent agreement with Eq. (36) for $|\bar{x}| < 1$. Note that the coefficients of the quadratic term in Eq.(36) are very small. In particular, since $|\bar{x}| < 1$, the thickness of the liquid film is approximately constant inside the “contact” zone and is given by $c(\beta)$, the thickness where the pressure gradient is exactly zero.

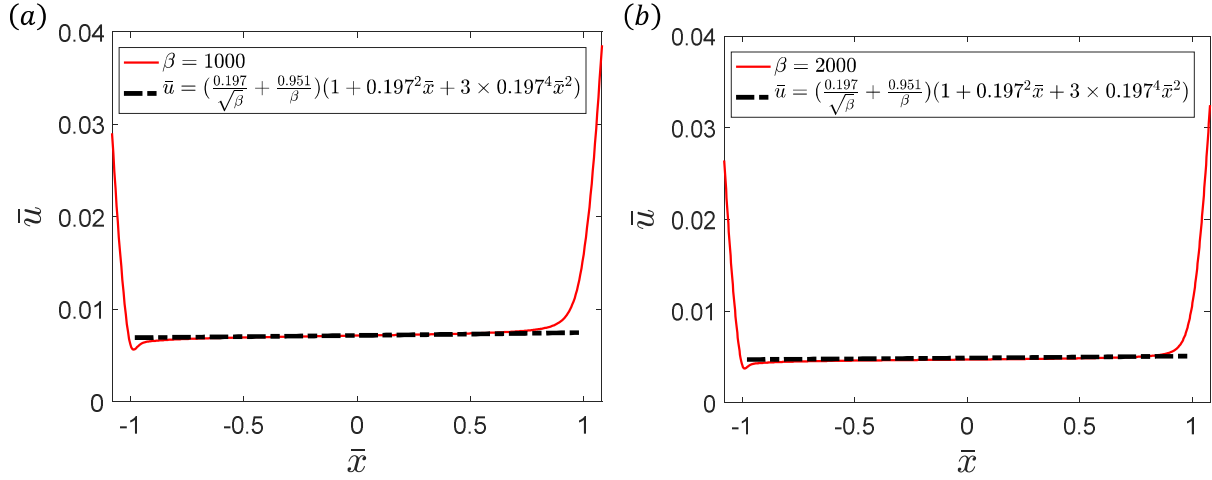


Fig.5 Comparison of the film thickness profile with Eq. (36) for two different β values: (a) $\beta=1000$ and (b) $\beta=2000$.

3. Numerical method of solving full v-EHL problem

In this section, we highlight a numerical method to solve the v-EHL lubrication problem which requires simultaneously solving the Reynolds equation and for the surface deformation. In the literature, the Reynolds equation for the sliding problem is usually solved using either relaxation [36, 37] or Newton-Raphson methods [43, 44]. In this work, we used a forward relaxation method [25] which is easier to implement and less memory-demanding compared with the Newton-Raphson method. The numerical method here differs from previous work [36] in two aspects: we consider viscoelasticity and using a normal force condition. Calculation of the deformation of the viscoelastic material requires extra computation time as the deformation depends not only the spatial distribution of the load but also the loading history. In the previous section, we have shown that this difficulty can be bypassed by integrating the temporal integrand analytically which results in an expression involving only the spatial integrand. This allows efficient evaluation of the viscoelastic deformation. As mentioned previously, the absolute surface deformation is not well defined, which makes a displacement control loading scheme physically nonintuitive. Instead, we applied normal force control which requires us to find the relative position of the cylinder, h_0 . This position is determined by the condition that the pressure satisfies Reynold's equation and normal force balance.

We use a central difference scheme to discretize the first and second derivatives in Eq.(10), i.e.,

$$\left(\frac{\partial f}{\partial \bar{x}}\right)_i = \frac{f_{i+1} - f_{i-1}}{2\Delta\bar{x}}; \left(\frac{\partial^2 f}{\partial \bar{x}^2}\right)_i = \frac{f_{i+1} - 2f_i + f_{i-1}}{(\Delta\bar{x})^2} \quad (37)$$

Using Eq.(37), the discretized form of Eq.(10) becomes:

$$A_i \bar{p}_{i-1} + B_i \bar{p}_i + C_i \bar{p}_{i+1} = D_i \quad (38)$$

$$\text{where: } A_i = \left[\frac{(\bar{u}_i)^2}{(\Delta\bar{x})^2} \left(\frac{3}{4}\bar{u}_{i-1} + \bar{u}_i - \frac{3}{4}\bar{u}_{i+1} \right) \right]; \quad B_i = -2 \frac{(\bar{u}_i)^3}{(\Delta\bar{x})^2};$$

$$C_i = \left[\frac{(\bar{u}_i)^2}{(\Delta\bar{x})^2} \left(-\frac{3}{4}\bar{u}_{i-1} + \bar{u}_i + \frac{3}{4}\bar{u}_{i+1} \right) \right]; \quad D_i = -\frac{\bar{u}_{i+1} - \bar{u}_{i-1}}{2\beta\Delta\bar{x}};$$

The discretized form of film thickness is $\bar{u}_i = \bar{h}_i - \bar{w}_i$, where \bar{h}_i and \bar{w}_i are the position of the cylinder's surface and the substrate surface's deformation at \bar{x}_i . They are computed according to

$$\bar{h}_i = \bar{h}_0 + \frac{1}{2}\bar{x}_i^2 \quad (39)$$

$$\bar{w}_i = \sum_{k=1}^n \chi_{ik}(\bar{x}_i, \bar{x}_k) \bar{p}_k \quad (40)$$

$$\chi_{ik} = \left[\frac{1}{\pi} \ln \left| \frac{\bar{x}_i - \bar{x}_k}{\bar{r}_0 - \bar{x}_k} \right| - \frac{f}{\pi(1+f)} e^{\alpha(\bar{x}_i - \bar{x}_k)} Ei(-\alpha(\bar{x}_i - \bar{x}_k)) \right] \cdot \Delta\bar{x} \quad (41)$$

Note Eq.(40) is Eq.(17) in discretized form, where n is the total number of grid points. The discretized form of the Reynolds equation Eq.(10) is solved using forward relaxation method where \bar{p}_i^{curt} in the current iteration is related to the previous iteration \bar{p}_i^{prev} by:

$$\bar{p}_i^{curt} = \bar{p}_i^{prev} + \lambda_p \left(D_i - A_i \bar{p}_{i-1}^{curt} - B_i \bar{p}_i^{prev} - C_i \bar{p}_{i+1}^{prev} \right) / B_i \quad (42)$$

In Eq.(42), λ_p is the relaxation factor which controls the convergence rate of the relaxation iteration. Large λ_p usually results in faster convergence. However, it is also less stable and iteration is more prone to diverge. In our calculations, we found the values of λ_p which optimize convergence rate and stability falls in a relatively large range, $\lambda_p = 0.01 - 0.8$. The relaxation factor also depends on the choice of parameters α , f and β . Usually, small α and large f , β values require smaller λ_p to ensure stable convergence.

Once the hydrodynamic pressure is found using the above scheme, we need to check if the normal force balance Eq.(12) is satisfied. The discretized form of Eq.(12) is:

$$\sum_{i=1}^n \bar{p}_i \Delta\bar{x} = \frac{\pi}{2}. \quad (43)$$

If normal force balance is not satisfied, the film thickness is either too large or too small and the position of the cylinder, \bar{h}_0 , should be adjusted. In our numerical scheme, \bar{h}_0 is updated every n_h iterations using

$$\bar{h}_0^{curt} = \bar{h}_0^{prev} + \lambda_{h1} \left| 1 - \frac{2}{\pi} \sum_{i=1}^n \bar{p}_i^{curt} \Delta\bar{x} \right| + \lambda_{h2} \frac{\|\bar{p}^{curt} - \bar{p}^{prev}\|}{\|\bar{p}^{prev}\|} \quad (44)$$

In Eq.(44), the adjustment of \bar{h}_0 includes two parts: the normalized normal force balance residual and the relative change of pressure in two iterations. Even though \bar{h}_0 is directly related to normal force balance, we found that including the contribution of the pressure change is very important for convergence when $\alpha < 0.1$. The parameters λ_{h1} , λ_{h2} are relaxation factors associate with these two residuals. In our calculation, λ_{h1} is found to be in the range of 0.001–0.01 and $\lambda_{h2}=10-20$ for $\alpha \ll 1$ while $\lambda_{h2}=0$ works well for $\alpha \geq 1$. Note that smaller n_h allows prompt adjustment of the cylinder position which potentially helps faster convergence. However, the iteration could become more unstable. We have found that an appropriate n_h is in the range of 10 – 200 .

A flow chat of the numerical scheme is shown in Fig.6. An initial guess of the pressure profile \bar{p}^{init} and \bar{h}_0^{init} has to be provided to start the iteration. \bar{p}^{init} , \bar{h}_0^{init} are chosen to be the corresponding EHL solution with the target β value. Note that a good initial guess is critical for the iteration to converge in a fast and stable pace.

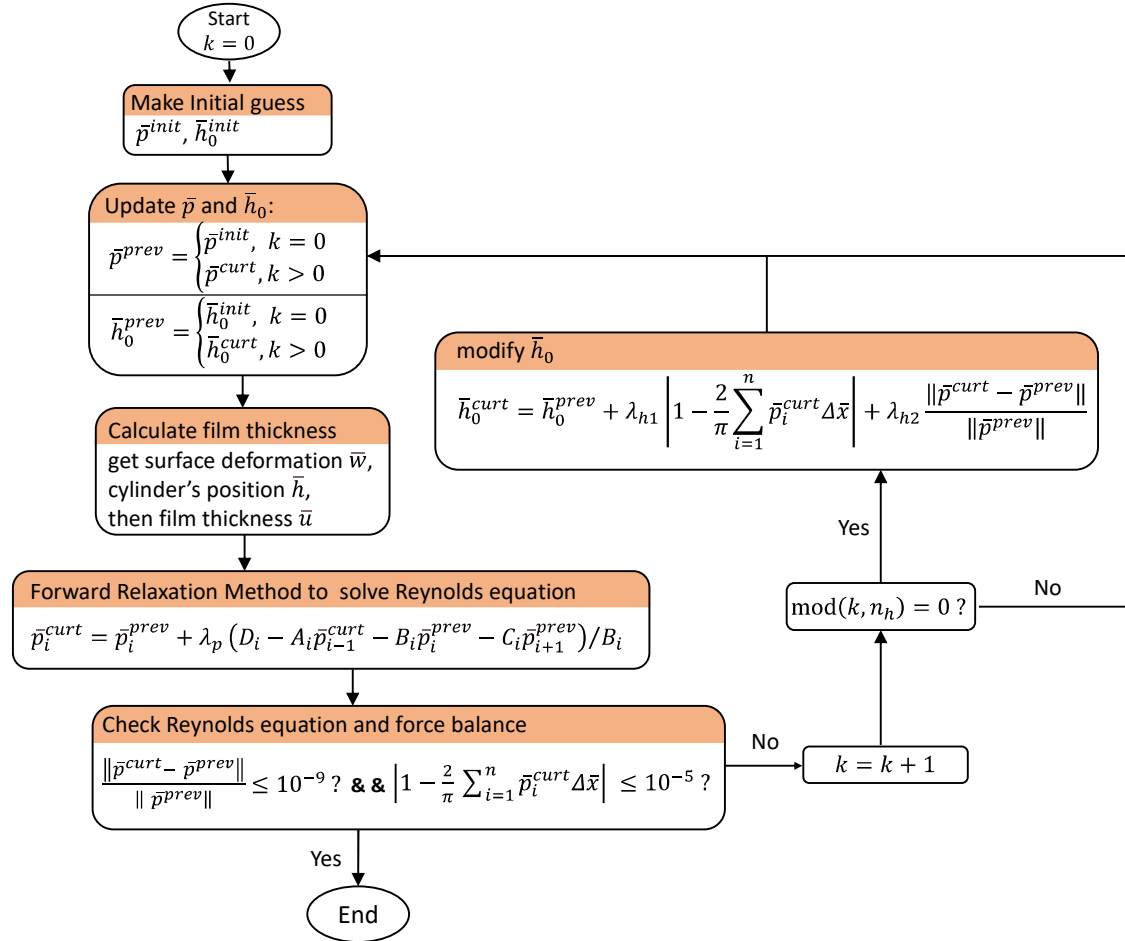


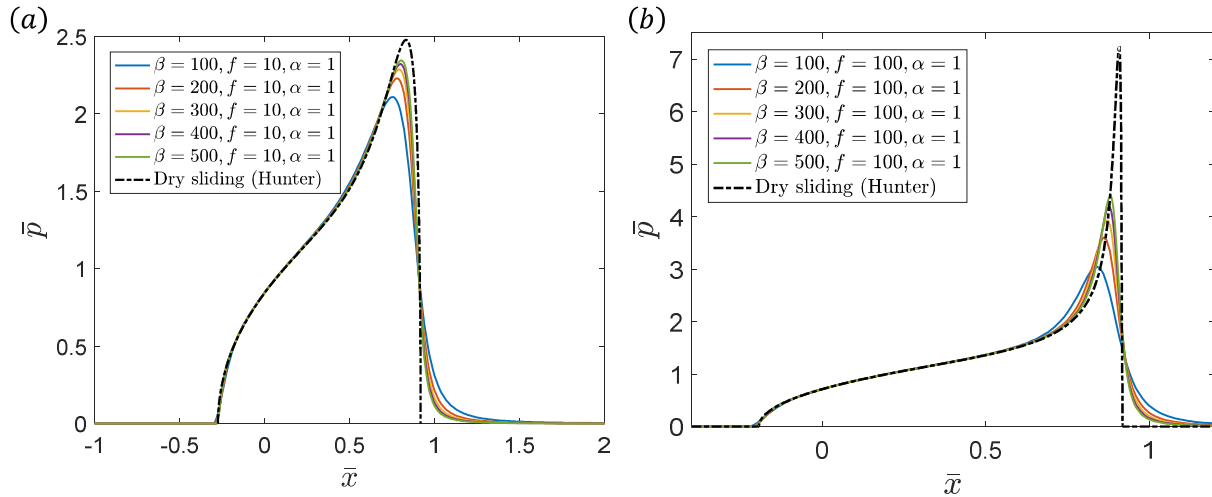
Fig.6 A flow chat summarizing the numerical scheme for solving Eqs.(10-12). For detailed description, see text above and Eqs. (37) to (44).

4. Numerical Results of the v-EHL problem

4.1 Hydrodynamic pressure and Substrate deformation

Figure 7a,b,c plot the normalized hydrodynamic pressure distribution $\bar{p}(\bar{x})$ for different combinations of α, β and f . The colored lines are the numerical results obtained by solving Eqs.(10-12). The black dashed lines are the dry sliding results from Eq.(24). Note $\alpha = 1$ in both Fig. 7a and 7b with f changing from 10 (Fig. 7a) to 100 (Fig.7b). Recall that $f = E_0/E_\infty - 1$ so a larger f indicates stronger viscoelasticity. Here we focus on highly viscoelastic solids such as rubber where $f \approx 100$ or higher. Figure 7a and 7b show that the hydrodynamic pressure peaks near the leading edge since the strain rate is highest here. Also, as β increases, the hydrodynamic pressure approaches the dry sliding contact pressure. This is reasonable, since larger β corresponds to higher normal loads or smaller sliding velocities; both conditions result in a thinner film. The main difference between the dry solution and the v-EHL solution is near the leading edge, where the pressure of the dry solution drops abruptly to zero.

Figure 7c fixes β and f while varying α by 6 orders of magnitude. Recall that $\alpha = a_0/V\tau$ is the ratio of time to slide the cylinder over half Hertzian contact width over the characteristic retardation time of the viscoelastic material. This figure shows that the hydrodynamic pressure is well approximated by the dry sliding pressure for all α values. The pressure is highly skewed for $\alpha = 0.1$ and 1: pressure is concentrated at the leading edge. This means that if the time for the cylinder to slide over half the Hertzian contact width is comparable to the retardation time, the front half of the cylinder will experience much higher hydrodynamic pressure. For very large and small α , the pressure is given by the elastic solution (Hertz pressure) corresponding to a relaxed or stiff substrate with modulus E_∞^* and E_0^* respectively.



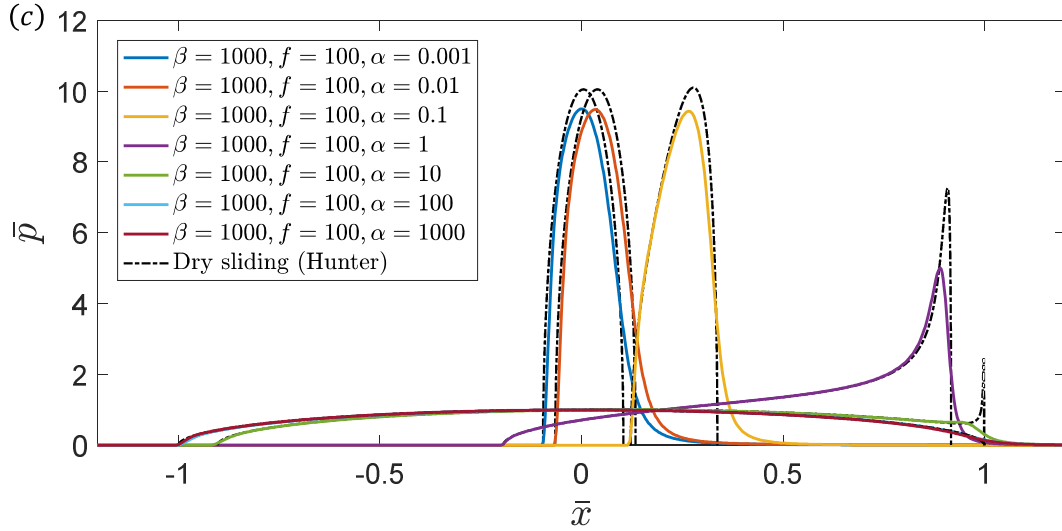


Fig.7 Comparison of the hydrodynamic pressure profile with the dry sliding pressure Eq.(24). (a) $\alpha=1$, $f=10$, $\beta=100-500$; (b) $\alpha=1$, $f=100$, $\beta=100-500$; (c) $\beta=1000, f=100$, α varies from 10^{-3} to 10^3 . In (a,b,c), the dry sliding pressure cases are shown by the black broken lines.

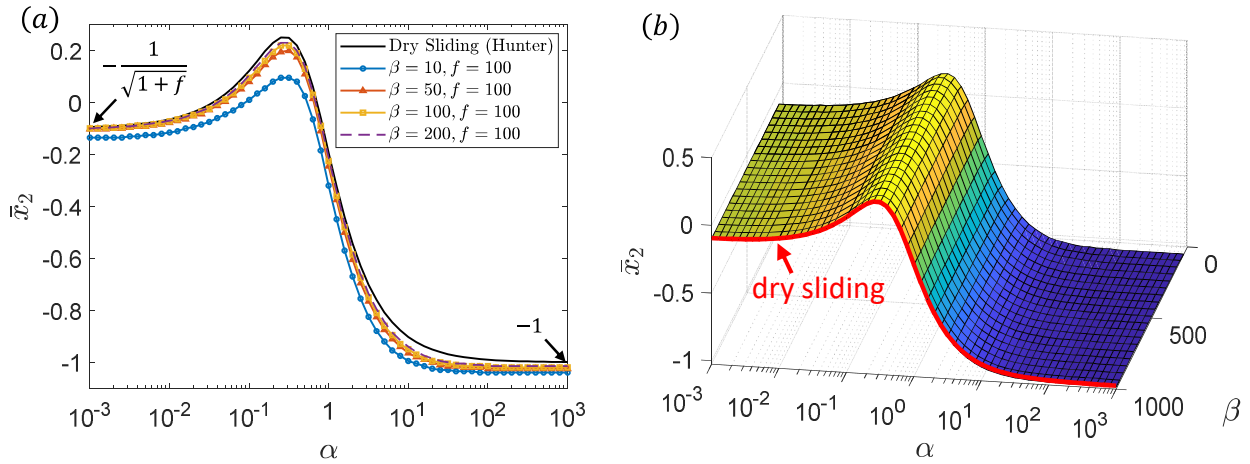


Fig.8 Comparison of the trailing edge position \bar{x}_2 with the dry sliding prediction. (a) $\beta=10,50,100,200$ (b) $\beta=10-1000$. Results show that for $\alpha = 0.1-1$, the rear position of the effective contact is larger than 0 which indicates that the hydrodynamic pressure concentrates in the region $\bar{x} > 0$.

Figures 8a,b plot the position of the trailing edge \bar{x}_2 which is *defined* as the location where pressure first approaches zero. Here it is important to note that in our numerical calculation, the Reynolds condition [36] is applied to eliminate regions of negative pressure. In these figures, $f=100$ and β varies from 10 to 1000. The horizontal axis is α which varies from 10^{-3} to 10^3 . In the same figure, we also

present the trailing edge of the dry sliding solution, \bar{x}_2 which is obtained from Eqs. (26, 29, 30). Figure 8c shows that as β increases, \bar{x}_2 approaches the dry sliding limit. It is interesting to note that $\bar{x}_2 > 0$ for $\alpha \in (0,1)$. In this range of α , the material is highly dissipative and hydrodynamic pressure is concentrated in the front part of the cylinder (see also Fig. 7b,c). This skew pressure distribution can cause significant stress concentration at the leading edge as we shall see in Fig.9.

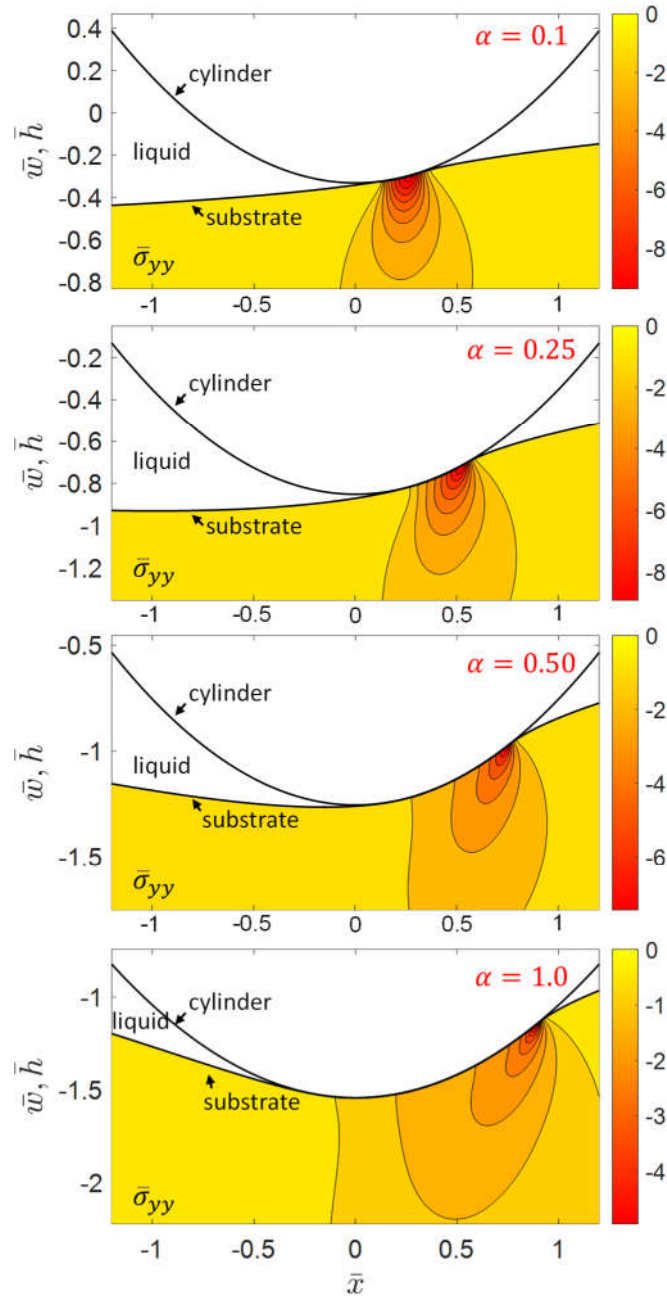


Fig.9 The deformed viscoelastic substrate and the cylinder's position for different α with constant f and $\beta, f=100, \beta=1000$. Contour plots of $\bar{\sigma}_{yy}$ in the substrate are shown.

Figure 9 shows contour plots of the normal stress component $\bar{\sigma}_{yy}$ near the leading edge. The calculation of $\bar{\sigma}_{yy}$ is given in SI. We focus on the range of $\alpha \in (0.1, 1)$ where the pressure field is highly skewed. The result of the two limits where $\alpha \rightarrow 0$ and $\alpha \rightarrow \infty$ is given in the SI. In these two limits, the deformation of the substrate is almost symmetric and contour of $\bar{\sigma}_{yy}$ approaches to the Hertzian results with elastic moduli E_∞^* and E_0^* respectively. For $\alpha = 0.1 - 1.0$, this asymmetric deformation is caused by the hydrodynamic pressure being concentrated more locally at a smaller region. With the skewed substrate deformation and concentrated pressure, one expects much higher counterreaction force acting on the rigid cylinder as shown schematically in Fig. 2. This is the friction force due to the viscoelastic deformation, F_v .

4.2 Viscoelastic dissipation: Loading and unloading cycles and the viscoelastic friction force F_v

The expression for the friction force F_v , Eq.(22) can be interpreted as the viscoelastic energy dissipated as a material point entering the leading edge and exiting the trailing edge. As this point enters the leading edge, it is actively loaded and it unloads to zero pressure as it exits the trailing edge. Figure 10 shows this loading and unloading cycle for a typical material point on the substrate surface for $f=10, 100$. The dry limit results calculated using Eqs.(24) and (17) (black dotted lines) are also plotted in the same figure for comparison. The area enclosed by the loading and unloading curves is the dissipated energy, \bar{F}_v . In Fig. 10a,b, $\alpha = 1$, for which, we found numerically, the energy dissipation is approximately maximum. Results for a broad range of α are shown in Fig.11.

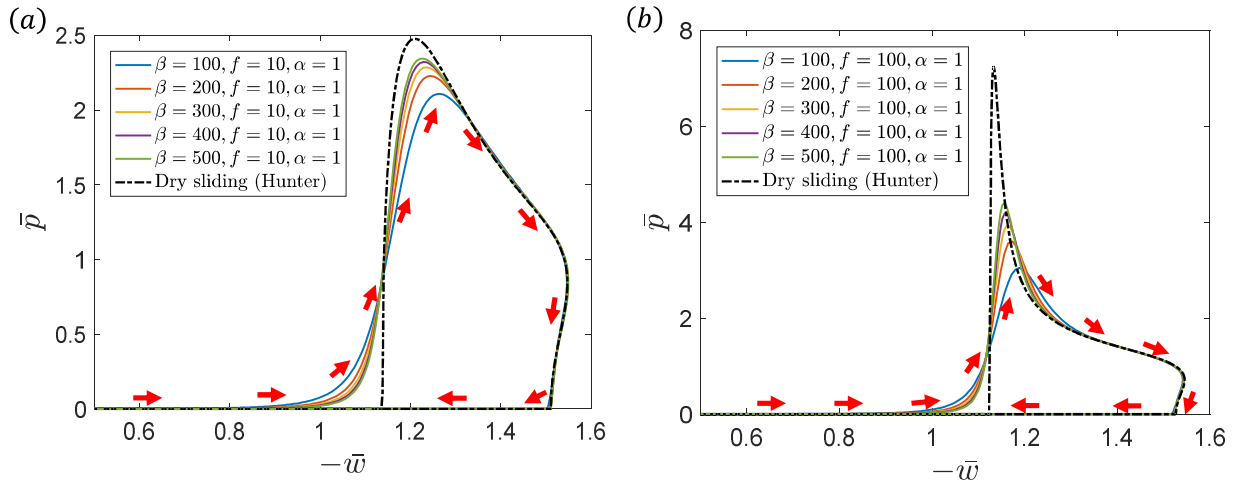


Fig.10 The loading and unloading cycles for a typical material point on the substrate's surface. Dry sliding solution is plotted in comparison. (a) $f=10$, (b) $f=100$. Different β values are plotted to show the trend of approaching the dry limit solution.

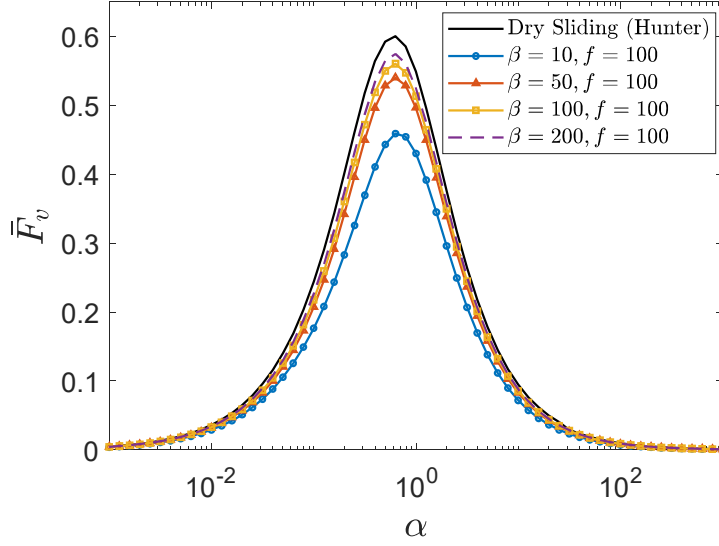


Fig. 11 Normalized friction force \bar{F}_v due to viscoelastic energy dissipation against α for different β . The dry sliding limit is the solid black line.

Figure 11 plots the normalized friction force due to viscoelastic energy dissipation versus α for different values of β . The black solid line is the dry sliding friction force calculated using Eq.(31). Note that the dissipation or friction force \bar{F}_v reaches the maximum at roughly $\alpha=1$ for different β . As expected, when \bar{F}_v approaches 0 when $\alpha \rightarrow 0$ or ∞ . In these limits, the substrate is elastic. *It is interesting to note that the dry sliding friction is an upper bound for \bar{F}_v .* This is because the liquid layer smooths out the skewed pressure distribution and hence reduces the friction force. The VEHL friction approaches the dry limit as β increases.

We summarize this section by emphasizing that the friction due to viscoelasticity of the substrate can be well approximated by the dry sliding solution and hence is effectively decoupled from the hydrodynamics for sufficiently large β . The situation is more complicated for the friction due to hydrodynamics since the gap size is expected to be sensitive to viscoelasticity. Nevertheless, the dry sliding solution can be exploited to determine this gap thickness, and this feature allows us to determine the hydrodynamic component of the friction force without solving the full lubrication problem, as we shall demonstrate below.

4.3 Liquid film thickness and hydrodynamic friction force F_h

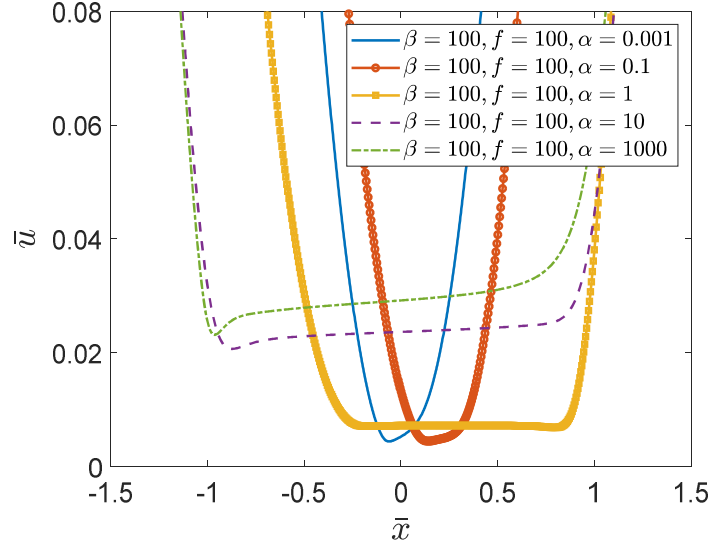


Fig.12 Film thickness profile for a large range of α values.

Figure 12 plots the liquid film thickness profile for different α values while fixing β, f . The liquid film thickness increases with α and varies by about an order of magnitude. This is not surprising since large α implies that the substrate underneath the cylinder is relaxed, with long time modulus. Indeed, as α decreases, the substrate underneath the cylinder becomes effectively stiffer, and this decreases the size of the “effect contact zone”. To support the higher normal load, the liquid film thins to increase the hydrodynamic pressure.

To incorporate the effect of α and f into the hydrodynamic friction, we note that the scaling $c \approx O(1/\sqrt{\beta})$ and $\bar{u} \approx O(1/\sqrt{\beta})$ still holds for the VEHL case at large β value except that c and \bar{u} now depends not only β , but also on α and f . Integrating of Eq.(6a) yields:

$$\beta \bar{p}_{, \bar{x}} \bar{u}^3 = -\bar{u} + c(\beta, \alpha, f) \quad (45)$$

where c takes the form of:

$$c = \frac{\rho_1(\alpha, f)}{\sqrt{\beta}} + \frac{\rho_2(\alpha, f)}{\beta} \quad (46)$$

From our previous calculation of EHL in 2.2.2, we found:

$$\rho_1(\alpha \rightarrow \infty, f) = 0.197, \quad \rho_2(\alpha \rightarrow \infty, f) = 0.951 \quad (47)$$

$$\rho_1(\alpha \rightarrow 0, f) = \frac{0.197}{\sqrt{1+f}}, \quad \rho_2(\alpha \rightarrow 0, f) = \frac{0.951}{1+f} \quad (48)$$

We also have $\rho_1(\alpha, f=0)=0.197$, $\rho_2(\alpha, f=0)=0.951$ which are the elastic limits. A plot for c versus β for $f=100$ for different α is shown in the Fig. 13 where the symbols are the numerical c values. The solid lines in Fig.13 are calculated using the expression:

$$c = \frac{0.197}{\sqrt{\beta^*}} + \frac{0.951}{\beta^*} \quad \text{where } \beta^* \equiv \beta(1 + fe^{-1.41\alpha}) \quad (49)$$

Figure 13 shows that Eq.(49) captures the numerical results well. This equation allows us to approximately determine the film thickness in the full viscoelastic sliding problem, as will be demonstrated below.

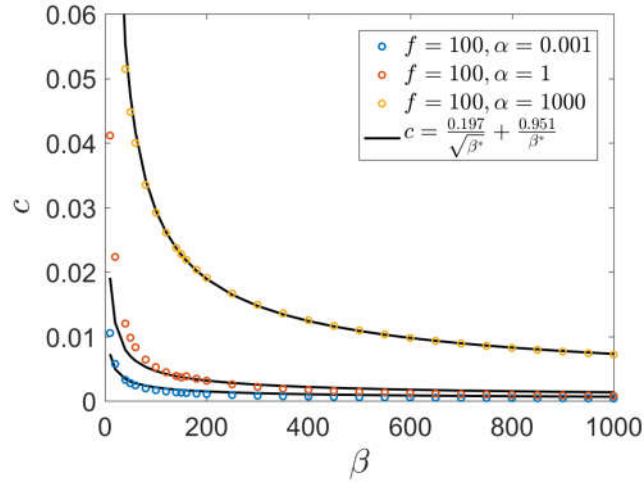


Fig.13 Numerical result of c versus β for different α values (symbols). The solid black lines are calculated using by Eq.(24) .

As shown in the previous section, for $\beta \geq 50$, the dry limit of \bar{p} obtained from Eq.(24) is a good approximation for the hydrodynamic pressure. *Using the dry limit of \bar{p} , we can solve the cubic equation Eq.(45) with c given by Eq.(49) for \bar{u} . This procedure allows us to determine the fluid film thickness in the “contact” zone for large β . The result of the asymptotic solution of \bar{u} (for large β) is shown as symbols in Fig. 14(a) and the full solution of \bar{u} is shown as solid lines for comparison.*

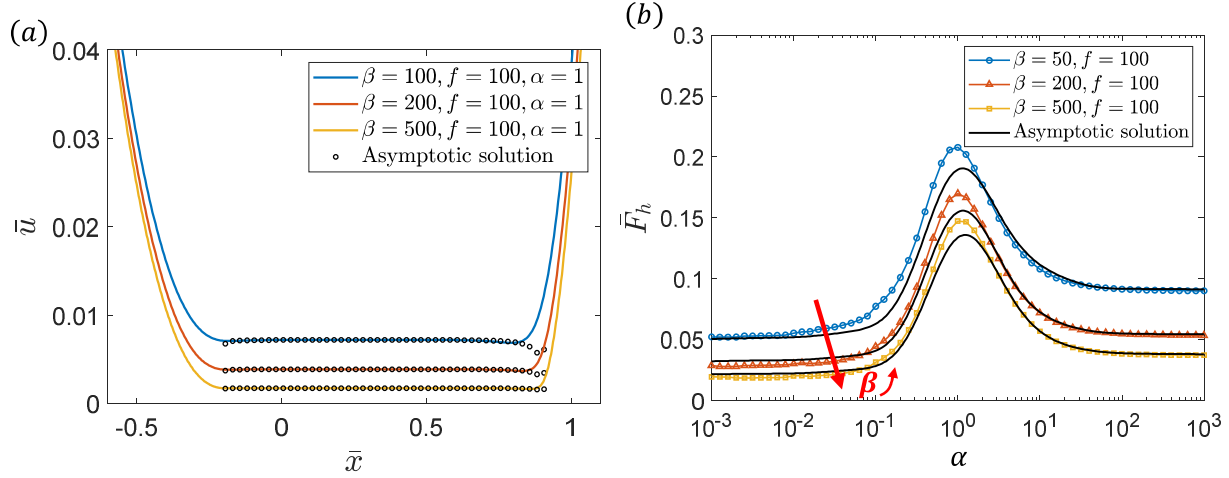


Fig.14 (a) Comparison of VEHL solution with asymptotic solution for the film thickness profile. The asymptotic solution is obtained by solving the cubic equation, Eq.(45) with c given by Eq.(49) and P given by Eq.(24). (b) The normalized hydrodynamic friction force \bar{F}_h versus α . Asymptotic solutions of \bar{F}_h calculated by using the dry limit of \bar{p} and the asymptotic solution of \bar{u} are shown in black solid lines.

The above analysis demonstrates an important result: *the hydrodynamic friction Eq.(18) can be determined using the dry sliding pressure and the gap thickness determined using the dry pressure and solving a cubic*. The validity of this approximate solution is checked by comparing the solution of the full VEHL problem in Fig. 14b. In Fig.14(b) we plot the normalized hydrodynamic friction force \bar{F}_h for a large range of α . \bar{F}_h is calculated using Eq.(20). The black solid lines are the approximation solutions. For all practical purposes, the proposed approximation works. Both numerical and approximate solutions show that \bar{F}_h decreases with increasing β . For small α , $\alpha < 0.1$ and large α , $\alpha > 10$, \bar{F}_h plateaus indicating that \bar{F}_h is insensitive to α as the elastic limits are approached. As expected, \bar{F}_h peaks at $\alpha \approx 1$ for different β .

4.4 Total friction in viscoelastic lubrication and generalized Stribeck surface

The total friction force F_{tot} is the sum of the viscoelastic friction F_v and the hydrodynamic friction F_h . Using our approximation, F_{tot} and the corresponding friction coefficient μ_{tot} are:

$$F_{tot} = F_v + F_h = \frac{Na_0}{R} \left[\left(\bar{b} - \frac{1}{\alpha(1+f)} - \bar{a}^3 \bar{\Gamma}_1 \right) + \int_{-\infty}^{\infty} \left(\frac{\bar{p}_{,x} \bar{u}}{\pi} + \frac{1}{3\pi\beta\bar{u}} \right) d\bar{x} \right] \equiv \frac{Na_0}{R} \bar{F}_{tot} \quad (50)$$

$$\mu_{tot} = \frac{F_{tot}}{N} = \frac{a_0}{R} \left[\left(\bar{b} - \frac{1}{\alpha(1+f)} - \bar{a}^3 \bar{\Gamma}_1 \right) + \int_{-\infty}^{\infty} \left(\frac{\bar{p}_{,x} \bar{u}}{\pi} + \frac{1}{3\pi\beta\bar{u}} \right) d\bar{x} \right] = \mu_v + \mu_h \quad (51)$$

where \bar{a} , \bar{b} , $\bar{\Gamma}_1$ are defined in Eq.(26, 29, 27), \bar{p} is given by Eq.(24) and u is determined from the solution of the cubic Eq.(45).

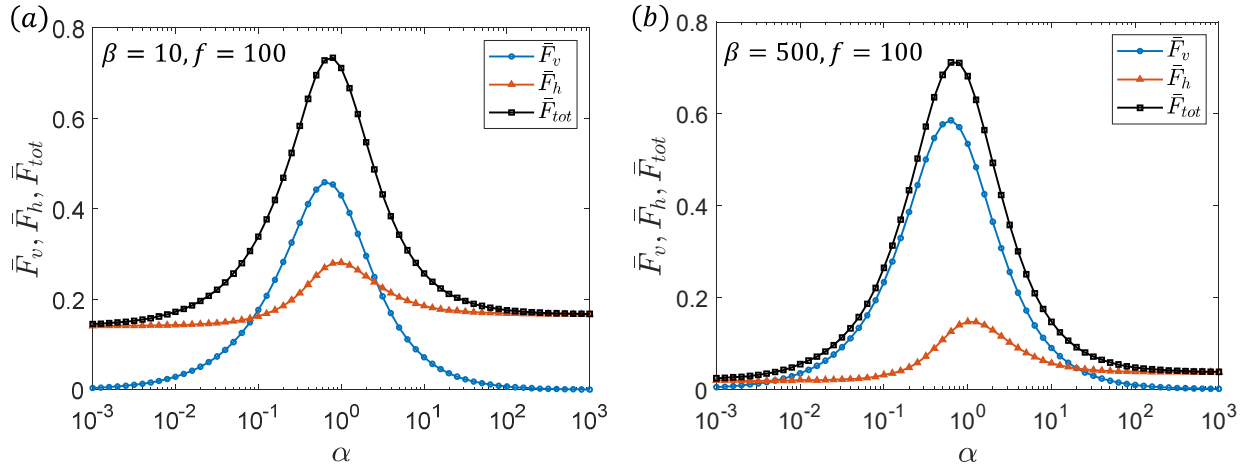
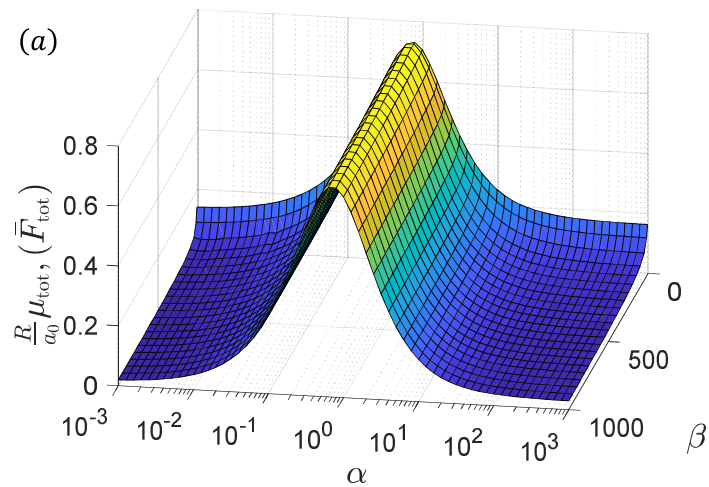


Fig.15 Total friction force \bar{F}_{tot} versus α for $f=100$, (a) $\beta=10$, (b) $\beta=500$. The components of \bar{F}_h and \bar{F}_v are also shown for comparison.

Figure 15 plots the total friction force \bar{F}_{tot} (black line) against large range α , $\alpha=10^{-3} \sim 10^3$. Also plotted are the viscoelastic friction \bar{F}_v (blue line) and the hydrodynamic friction \bar{F}_h (red line). For very small $\alpha < 0.1$ and very large $\alpha > 10$ (i.e. very fast and very small loading rate), the total friction is mainly contributed by hydrodynamics as the substrate is elastic and no viscoelastic energy is dissipated. For moderate loading rates, $\alpha = 0.1 - 10$, the viscoelastic friction \bar{F}_v kicks in and contribute significantly to the total friction force. Comparing Fig.15(a) and (b) shows that as β increases viscoelastic dissipation is the dominant friction mechanism. In this regime, the calculation is much simpler since \bar{F}_v is completely determined by the dry friction solution.



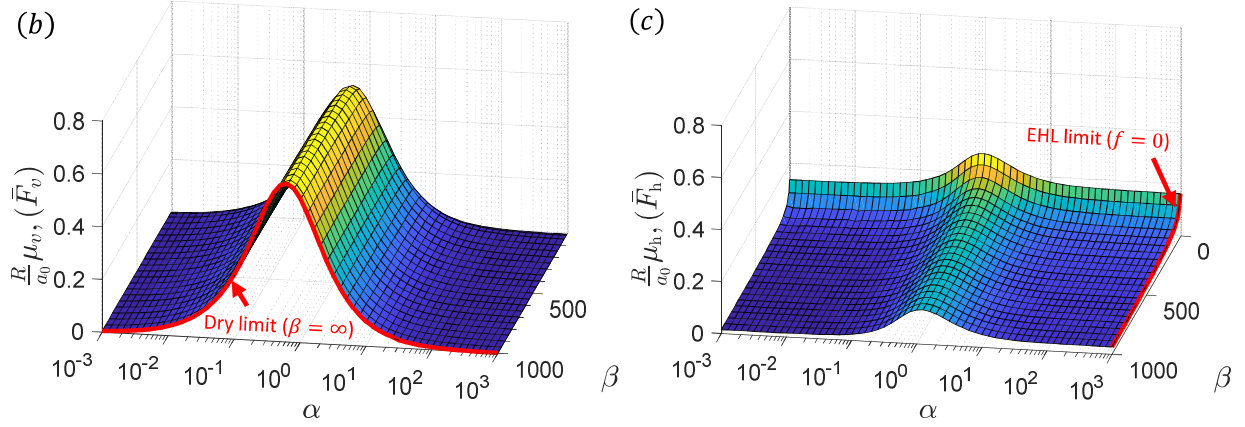


Fig.16 Generalized Stribeck surfaces. (a) total friction coefficient μ_{tot} versus α, β . (b-c): viscoelastic friction coefficient μ_v and hydrodynamic friction coefficient μ_h versus α, β .

In the EHL regime, it is common practice to use the Stribeck curve where the friction coefficient is plotted against the Hersey number. However, it must be noted that, even for an elastic substrate, the solution of the sliding problem *cannot be expressed solely in terms of the Hersey number*. Indeed, as shown above and by others [34, 45, 46], friction depends on the parameter β , which can be viewed as a generalized inverse Hersey number. Substrate viscoelasticity complicates the analysis as friction coefficient depends not only on β , but also on α and f . Thus, the generalization of the Stribeck curve is a Stribeck surface in the 4 dimensional space $(\alpha, \beta, f, \mu_{tot})$. Here, we present a slice of this 4 dimensional surface by fixing $f=100$. In Fig.16, we present 3D slices of the generalized Stribeck surfaces in $(\alpha, \beta, \mu_{tot}), (\alpha, \beta, \mu_v), (\alpha, \beta, \mu_h)$. Figure 16b shows that for large β , viscoelasticity controls the total friction force. The friction calculated using the dry sliding limit is shown in the same plot for comparison. However, for small α , $\alpha < 0.01$ and large α regions, $\alpha > 100$, the hydrodynamic friction force contributes significantly to the total friction as shown in Fig.16(c). The elastic lubrication limit is shown in the same plot for comparison.

5. Discussion and Summary

In this work, we studied the lubricated sliding of a rigid cylinder on a viscoelastic substrate with an emphasis on how substrate viscoelasticity affects sliding friction. We developed a robust numerical algorithm and used it to solve the full viscoelastic lubrication problem. Our theoretical formulation shows that whereas EHL is governed solely by the generalized inverse Hersey number β , the full viscoelastic lubrication solution depends on two extra dimensionless parameters: α and f . The parameter α represents ratio of time taken to traverse the contact region to the characteristic viscoelastic relaxation time; f is the ratio of short and long-time moduli (minus one) denoting the strength of viscoelasticity.

Our analysis suggests an approach that can further simplify the problem. We find that many results of the full viscoelastic lubrication problem can be obtained by the combination of two simpler limiting cases. The first of these is the dry sliding limit in which the liquid layer is absent – the cylinder and viscoelastic substrate are in direct contact. The second one is the elastic lubrication limit in which the viscoelastic substrate is replaced by an elastic material. We have examined these two limits in detail. Our results show that the dry sliding contact pressure distribution is usually a good approximation of the hydrodynamic pressure in the lubricated case, especially in the large β regime. The liquid film thickness can be calculated approximately using perturbation theory together with the dry contact pressure. The viscoelastic friction force due to viscoelastic energy dissipation dominates the total friction in this large β regime. For small α regime, $\alpha < 0.01$, and large α regime, $\alpha > 100$, the hydrodynamic friction is the main source for the total friction. The dry limit solution summarized in this work, the scaling analysis for the elastic lubrication and the numerical scheme proposed for the full viscoelastic lubrication problem could be useful in other similar work. Also, the substrate is assumed to be standard viscoelastic solid in current work. One can linearly combine more characteristic retardation time into the model to fully approximate more realistic creep behavior of soft matter using similar methodology shown in this work.

Supplementary Information The online version of this article contains supplementary material, which is available to authorized users.

Acknowledgements This work was supported by the National Science Foundation, through a LEAP-HI/GOALI grant, CMMI-1854572.

Declarations

Conflict of interest The authors declare that they have no competing interest.

Consent to Publish All authors have seen the manuscript and approved to submit to the journal, and we would greatly appreciate for your attention and consideration.

References

1. Okrent, E.H.: The effect of lubricant viscosity and composition on engine friction and bearing wear. *ASLE Transactions*. 4, 97–108 (1961). <https://doi.org/10.1080/05698196108972423>
2. Tzeng, S.T., Saibel, E.: Surface roughness effect on slider bearing lubrication. *ASLE Transactions*. 10, 334–348 (1967). <https://doi.org/10.1080/05698196708972191>
3. Martz, B.L.S.: Preliminary Report of Developments in Interrupted Surface Finishes. *Proceedings of the Institution of Mechanical Engineers*. 16, 1–9 (1947). <https://doi.org/10.1111/j.1559-3584.1950.tb02844.x>
4. Mcgeehan, J.A.: A Literature Review of the Effects of Piston and Ring Friction and Lubricating Oil Viscosity on Fuel Economy. In: *SAE Technical Paper Series* (1978)

5. Ioannides, E.: EHL in rolling element bearings, recent advances and the wider implications. In: Tribology Series. pp. 3–14. Elsevier (1997)
6. Liu, X.L., Song, D.T., Yang, P.R.: On Transient EHL of a Skew Roller Subjected to a Load Impact in Rolling Bearings. *KEM*. 739, 108–119 (2017).
<https://doi.org/10.4028/www.scientific.net/KEM.739.108>
7. Persson, B.N.J., Albohr, O., Tartaglino, U., Volokitin, A.I., Tosatti, E.: On the nature of surface roughness with application to contact mechanics, sealing, rubber friction and adhesion. *J. Phys.: Condens. Matter*. 17, R1–R62 (2005). <https://doi.org/10.1088/0953-8984/17/1/R01>
8. Thatte, A., Salant, R.F.: Elastohydrodynamic Analysis of an Elastomeric Hydraulic Rod Seal During Fully Transient Operation. *Journal of Tribology*. 131, 031501 (2009).
<https://doi.org/10.1115/1.3139057>
9. Hamrock, B.J., Schmid, S.R., Jacobson, B.O.: Fundamentals of fluid film lubrication. Marcel Dekker, New York (2004)
10. Ludema, K.C., Ajayi, L.: Friction, wear, lubrication: a textbook in tribology. Taylor & Francis, CRC Press, Boca Raton (2019)
11. Bongaerts, J.H.H., Fourtouni, K., Stokes, J.R.: Soft-tribology: Lubrication in a compliant PDMS-PDMS contact. *Tribology International*. 40, 1531–1542 (2007).
<https://doi.org/10.1016/j.triboint.2007.01.007>
12. de Vicente, J., Stokes, J.R., Spikes, H.A.: The Frictional Properties of Newtonian Fluids in Rolling–Sliding soft-EHL Contact. *Tribol Lett*. 20, 273–286 (2005). <https://doi.org/10.1007/s11249-005-9067-3>
13. Selway, N., Chan, V., Stokes, J.R.: Influence of fluid viscosity and wetting on multiscale viscoelastic lubrication in soft tribological contacts. *Soft Matter*. 13, 1702–1715 (2017).
<https://doi.org/10.1039/C6SM02417C>
14. Rivetti, M., Bertin, V., Salez, T., Hui, C.-Y., Linne, C., Arutkin, M., Wu, H., Raphaël, E., Bäümchen, O.: Elastocapillary levelling of thin viscous films on soft substrates. *Physical Review Fluids*. 2, (2017).
<https://doi.org/10.1103/PhysRevFluids.2.094001>
15. Moyle, N., He, Z., Wu, H., Hui, C.-Y., Jagota, A.: Indentation versus Rolling: Dependence of Adhesion on Contact Geometry for Biomimetic Structures. *Langmuir*. 34, 3827–3837 (2018).
<https://doi.org/10.1021/acs.langmuir.8b00084>
16. Wu, H., Moyle, N., Jagota, A., Khripin, C.Y., Bremond, F., Hui, C.-Y.: Crack propagation pattern and trapping mechanism of rolling a rigid cylinder on a periodically structured surface. *Extreme Mechanics Letters*. 29, 100475 (2019). <https://doi.org/10.1016/j.eml.2019.100475>
17. Kim, J.M., Wolf, F., Baier, S.K.: Effect of varying mixing ratio of PDMS on the consistency of the soft-contact Stribeck curve for glycerol solutions. *Tribology International*. 89, 46–53 (2015).
<https://doi.org/10.1016/j.triboint.2014.12.010>
18. Sadowski, P., Stupkiewicz, S.: Friction in lubricated soft-on-hard, hard-on-soft and soft-on-soft sliding contacts. *Tribology International*. 129, 246–256 (2019).
<https://doi.org/10.1016/j.triboint.2018.08.025>
19. N. Moyle, F. Bremond, C.-Y. Hui, H. Wu, A. Jagota, C. Khripin, Material With Enhanced Sliding Friction (2021) U.S. Patent Application No. 20210283955.
<https://www.freepatentsonline.com/y2021/0283955.html>
20. Putignano, C.: Soft lubrication: A generalized numerical methodology. *Journal of the Mechanics and Physics of Solids*. 134, 103748 (2020). <https://doi.org/10.1016/j.jmps.2019.103748>
21. Hunter, S.C.: The Rolling Contact of a Rigid Cylinder With a Viscoelastic Half Space. *Journal of Applied Mechanics*. 28, 611 (1961). <https://doi.org/10.1115/1.3641792>

22. Carbone, G., Putignano, C.: A novel methodology to predict sliding and rolling friction of viscoelastic materials: Theory and experiments. *Journal of the Mechanics and Physics of Solids*. 61, 1822–1834 (2013). <https://doi.org/10.1016/j.jmps.2013.03.005>
23. Putignano, C., Reddyhoff, T., Carbone, G., Dini, D.: Experimental Investigation of Viscoelastic Rolling Contacts: A Comparison with Theory. *Tribol Lett.* 51, 105–113 (2013). <https://doi.org/10.1007/s11249-013-0151-9>
24. The relation between the friction and visco-elastic properties of rubber. *Proc. R. Soc. Lond. A*. 274, 21–39 (1963). <https://doi.org/10.1098/rspa.1963.0112>
25. Herrebrugh, K.: Solving the Incompressible and Isothermal Problem in Elastohydrodynamic Lubrication Through an Integral Equation. *Journal of Lubrication Technology*. 90, 262–270 (1968). <https://doi.org/10.1115/1.3601545>
26. Dowson, D., Higginson, G.R., Whitaker, A.V.: Elasto-Hydrodynamic Lubrication: A Survey of Isothermal Solutions. *Journal of Mechanical Engineering Science*. 4, 121–126 (1962). https://doi.org/10.1243/JMES_JOUR_1962_004_018_02
27. Hooke, C.J., Huang, P.: Elastohydrodynamic lubrication of soft viscoelastic materials in line contact. *Proceedings of the Institution of Mechanical Engineers, Part J: Journal of Engineering Tribology*. 211, 185–194 (1997). <https://doi.org/10.1243/1350650971542417>
28. Elsharkawy, A.A.: Visco-elastohydrodynamic lubrication of line contacts. *Wear*. 199, 45–53 (1996). [https://doi.org/10.1016/0043-1648\(96\)07212-2](https://doi.org/10.1016/0043-1648(96)07212-2)
29. Scaraggi, M., Persson, B.N.J.: Theory of viscoelastic lubrication. *Tribology International*. 72, 118–130 (2014). <https://doi.org/10.1016/j.triboint.2013.12.011>
30. Putignano, C., Dini, D.: Soft Matter Lubrication: Does Solid Viscoelasticity Matter? *ACS Appl. Mater. Interfaces*. 9, 42287–42295 (2017). <https://doi.org/10.1021/acsami.7b09381>
31. Putignano, C., Carbone, G., Dini, D.: Theory of reciprocating contact for viscoelastic solids. *Phys. Rev. E*. 93, 043003 (2016). <https://doi.org/10.1103/PhysRevE.93.043003>
32. Pandey, A., Karpitschka, S., Venner, C.H., Snoeijer, J.H.: Lubrication of soft viscoelastic solids. *J. Fluid Mech.* 799, 433–447 (2016). <https://doi.org/10.1017/jfm.2016.375>
33. Hui, C.-Y., Wu, H., Jagota, A., Khripin, C.: Friction Force During Lubricated Steady Sliding of a Rigid Cylinder on a Viscoelastic Substrate. *Tribol Lett.* 69, 30 (2021). <https://doi.org/10.1007/s11249-020-01396-5>
34. Persson, B.N.J.: *Sliding Friction*. Springer Berlin Heidelberg, Berlin, Heidelberg (2000)
35. Moyle, N., Wu, H., Khripin, C., Bremond, F., Hui, C.-Y., Jagota, A.: Enhancement of elastohydrodynamic friction by elastic hysteresis in a periodic structure. *Soft Matter*. 10.1039/C9SM02087J (2020). <https://doi.org/10.1039/C9SM02087J>
36. Wu, H., Moyle, N., Jagota, A., Hui, C.-Y.: Lubricated steady sliding of a rigid sphere on a soft elastic substrate: hydrodynamic friction in the Hertz limit. *Soft Matter*. 10.1039/C9SM02447F (2020). <https://doi.org/10.1039/C9SM02447F>
37. Hamrock, B.J., Dowson, D.: Isothermal Elastohydrodynamic Lubrication of Point Contacts: Part 1—Theoretical Formulation. *Journal of Lubrication Technology*. 98, 223 (1976). <https://doi.org/10.1115/1.3452801>
38. Gent, A.N., Lai, S.-M., Nah, C., Wang, C.: Viscoelastic Effects in Cutting and Tearing Rubber. *Rubber Chemistry and Technology*. 67, 610–618 (1994). <https://doi.org/10.5254/1.3538696>
39. Johnson, K.L.: *Contact Mechanics*. Cambridge University Press, Cambridge (1985)
40. Brandt, A., Lubrecht, A.A.: Multilevel matrix multiplication and fast solution of integral equations. *Journal of Computational Physics*. 90, 348–370 (1990). [https://doi.org/10.1016/0021-9991\(90\)90171-V](https://doi.org/10.1016/0021-9991(90)90171-V)
41. Biswas, S., Snidle, R.W.: Calculation of Surface Deformation in Point Contact EHD. *J. Lub. Tech.* 99, 313 (1977). <https://doi.org/10.1115/1.3453208>

42. Dowson, D., Hamrock, B.J.: Numerical Evaluation of the Surface Deformation of Elastic Solids Subjected to a Hertzian Contact Stress. *A S L E Transactions*. 19, 279–286 (1976). <https://doi.org/10.1080/05698197608982804>
43. Oh, K.P., Rohde, S.M.: Numerical solution of the point contact problem using the finite element method. *Int. J. Numer. Meth. Engng.* 11, 1507–1518 (1977). <https://doi.org/10.1002/nme.1620111003>
44. Rohde, S.M., Oh, K.P.: A Unified Treatment of Thick and Thin Film Elastohydrodynamic Problems by Using Higher Order Element Methods. *Proceedings of the Royal Society A: Mathematical, Physical and Engineering Sciences*. 343, 315–331 (1975). <https://doi.org/10.1098/rspa.1975.0068>
45. Snoeijer, J.H., Eggers, J., Venner, C.H.: Similarity theory of lubricated Hertzian contacts. *Physics of Fluids*. 25, 101705 (2013). <https://doi.org/10.1063/1.4826981>
46. de Vicente, J., Stokes, J.R., Spikes, H.A.: The Frictional Properties of Newtonian Fluids in Rolling–Sliding soft-EHL Contact. *Tribol Lett.* 20, 273–286 (2005). <https://doi.org/10.1007/s11249-005-9067-3>